A&A 626, A42 (2019)
https://doi.org/10.1051/0004-6361/201935246

Astronomy & Astrophysics

Polarimetric survey of main-belt asteroids

VII. New results for 82 main-belt objects[★,★★]

C. López-Sisterna, E. García-Migani, and R. Gil-Hutton

Grupo de Ciencias Planetarias, Departamento de Geofísica y Astronomía, Facultad de Ciencias Exactas, Físicas y Naturales, Universidad Nacional de San Juan - CONICET, Av. Ignacio de la Roza 590 (O), J5402DCS Rivadavia, San Juan, Argentina
e-mail: ricardo.gil-hutton@conicet.gov.ar

Received 11 February 2019 / Accepted 6 May 2019

ABSTRACT

Aims. We present the results of a polarimetric survey of main-belt asteroids at Complejo Astronómico El Leoncito (CASLEO), San Juan, Argentina. The aims of this survey are to increase the database of asteroid polarimetry and to estimate the diversity in the polarimetric properties of asteroids.
Methods. The survey began in 1995 and a second period began in 2013 using the CASPOL polarimeter with a more sensitive detector to study small asteroids, families, and special taxonomic groups. The data were obtained using this instrument at the 2.15 m telescope of CASLEO.
Results. We present 128 observations for 82 asteroids of different taxonomic types. These results revealed phase-polarization curves and polarimetric parameters for 20 asteroids, amounting to a total of 135 objects with sufficient good data in the Catalogue of Asteroid Polarization Curves. Using the values obtained for the objects with a taxonomic classification, we obtained the mean polarimetric parameters for 19 taxonomic types and the Barbarians. The asteroids with large mean scatter separation distances have a minimum of the phase-polarization curve greater than −1%, slopes at the inversion angle of less than 0.12–0.15% per degree, and perihelion distances $1.8 < q < 2.5$ au; these measurements indicate the asteroids could have high or moderate albedos and that they are objects with perihelia in the inner asteroid belt. These large mean scatter separation distance values could be the result of an electrostatic mechanism acting on the small grains of the regolith, a manifestation of a coherent backscattering mechanism, or the result of a surface formed by a mixture of dark and bright particles.

Key words. minor planets, asteroids: general – techniques: polarimetric

1. Introduction

The light that we receive from any asteroid at visible wavelengths consists of partially polarized light produced by the scattering of the sunlight on the solid surface of the body. The polarization is usually found to be linear with its azimuth either normal or parallel to the scattering plane, which in the solar system is the plane containing the asteroid, the Sun, and the Earth at the epoch of observation. In polarimetry, the results of observations are usually expressed using the parameter $P_r = (I_\perp - I_\parallel)/(I_\perp + I_\parallel)$, where $I_\perp$ and $I_\parallel$ are the intensities of the scattered light polarized along the planes perpendicular and parallel to the scattering plane, respectively.

The parameter P_r is affected by the composition, roughness, and other physical properties of the target and also depends on the illumination conditions. The variation of the degree of linear polarization as a function of the phase angle α, which is the angle between the directions to the Sun and to the observer as seen from the object, produces the so-called phase-polarization curve. This curve is described by some polarimetric parameters that provide information about the properties of the surface (Dollfus et al. 1989; Muinonen et al. 2002a; Kaasalainen et al. 2003). For phase angles $\lesssim 20°$, P_r turns out to be negative, reaching a minimum of polarization, P_{min}, at phase angles $\alpha_{min} \approx 6–12°$. Beyond $\approx 20°$ of phase, the polarization changes sign at the inversion angle, α_0, and becomes positive, increasing linearly for larger phase angles with a slope h.

Although polarimetry provides useful information about the physical properties of the asteroid surface, polarimetric observations of these objects are not easy to obtain because an asteroid must be followed at several phase angles to study its polarization curve; this kind of coverage is difficult owing to constraints such as object faintness, limited visibility, and weather problems. As a consequence, the database of asteroid polarimetric measurements was very small until about 1990 and very few objects had their polarimetric parameters well determined. Since 1995 we have made an extensive effort to conduct polarimetric observations at Complejo Astronómico El Leoncito (CASLEO), Argentina; the main objective has been to increase the available polarimetric database of main-belt asteroids. The first epoch of this survey ended in 2012 and a second epoch started in 2013 using new and more sensitive equipment. This survey provided a large number of polarimetric measurements of main-belt asteroids, including objects not observed before, and has the advantage of being a homogeneous dataset that has always been observed and reduced following the same procedures. These data, combined with results previously published, were used

[★] Table 1 is only available at the CDS via anonymous ftp to cdsarc.u-strasbg.fr (130.79.128.5) or via http://cdsarc.u-strasbg.fr/viz-bin/qcat?J/A+A/626/A42

[★★] Based on observations carried out at the Complejo Astronómico El Leoncito, operated under agreement between the Consejo Nacional de Investigaciones Científicas y Técnicas de la República Argentina and the National Universities of La Plata, Córdoba, and San Juan.

to obtain phase-polarization curves and polarimetric parameters of good quality for ≈120 main-belt asteroids[1] (Gil-Hutton & García-Migani 2017).

In this paper we report polarimetric observations obtained during 2017 and 2018, which have not yet been published, and we use these in combination with previously published data to find polarimetric parameters for several asteroids. In Sect. 2 we describe the observations, in Sect. 3 we present and discuss our results, and in Sect. 4 we draw our conclusions.

2. Observations

Our observations were carried out during various observing runs between April 2017 and November 2018 at the 2.15 m telescope of CASLEO using the CASPOL polarimeter. The CASPOL instrument is a polarization unit inserted in front of a CCD camera that allows high precision imaging polarimetry. This polarimeter was built following the design of Magalhaes et al. (1996), and uses an achromatic half-wave retarder and a Savart plate as an analyzer. The reduction and analysis of the images are done in the usual way using the Image Reduction and Analysis Facility (IRAF) tasks and scripts specially designed to reduce observations made with CASPOL[2]. The polarimetric parameters and errors are obtained from a least-squares solution to the measurements made at different half-wave plate positions. All the polarimetric measurements were made using a V-band filter.

From the analysis of several standard stars, we found the instrumental polarization to be fairly constant and stable, always below 0.05%. Whenever possible, we observed the targets during runs several weeks apart to obtain measurements during the same apparition at different phase angles. Observing nights were generally assigned around the new Moon to minimize the contamination of sky polarization by moonlight. Each night, we observed at least two zero-polarization standard stars and two high-polarization stars to determine instrumental polarization. The standard star data were obtained from Turnshek et al. (1990), Gil-Hutton & Benavidez (2003), and Fossati et al. (2007).

We observed the targets consecutively several times each night with individual exposure times long enough to reach signal-to-noise ratios (S/N) ≥ 40 in flux. Several measurements of each object were co-added to improve the S/N of the measurements at each position of the half-wave plate before obtaining the best fit to the polarization vector. The measurement errors were evaluated assuming a Poisson distribution and the final uncertainty was calculated through error propagation along the fitting process. After correcting for instrumental polarization, we obtained the Stokes parameters with reduction programs specifically designed for the CASPOL polarimeter; some modifications optimized the reduction to the specific needs of asteroid polarimetry. These optimizations included computations of the position angle of the scattering plane and polarization parameter P_r. The overall data reduction pipeline is essentially identical to that previously used in Gil-Hutton et al. (2017). As a test of the data reduction process, we analyzed the distribution of the ratio of the U component of linear polarization to its error and found that it is centered at zero, while all points differ from this value by less than a few σ, which supports the reliability of the polarimetric measurements.

[1] These data are available on the web page of the Grupo de Ciencias Planetarias at http://gcpsj.sdf-eu.org/catalogo.html

[2] The IRAF package for the CASPOL polarimeter is available at http://www.casleo.gov.ar

3. Results

During this period of the survey we obtained 128 observations for 82 main-belt asteroids. Each asteroid's name, date, total integration time in seconds (T_{int}), phase angle (α), position angle of the scattering plane ($\theta_\odot$), observed polarization (P) and its error (σ_P), position angle in the equatorial reference frame (θ) and its error (σ_θ), P_r, and Bus taxonomic classification (Bus 1999) taken from Bus & Binzel (2002) or Lazzaro et al. (2004) are listed in Table 1. For 6 asteroids the Bus type is not determined, therefore we used the taxonomic classification of Tholen (1989) and these asteroids are indicated with bold type in Table 1.

The data obtained for the asteroid (152) Atala confirm the overall shape of a phase-polarization curve with an inversion angle of ≈15° and a small P_{min}, which suggest a misclassification as a S-type object (Fornasier et al. 2006). The polarization values obtained for (678) Fredegundis in combination with previous published observations suggest that this object has significative variations in P_r, which could be a result produced by the change of the surface properties for different rotational phases. The asteroids (107) Camilla, (307) Nike, and (346) Hermentaria are observed for the first time.

With the data presented in this work it is possible to find polarimetric parameters for 20 asteroids not included previously in our Catalogue of Asteroid Polarization Curves[3], increasing to 135 the number of objects with phase-polarization curves of sufficient quality to find their polarimetric parameters. As usual, the phase-polarization curve was obtained by fitting the observations available for these objects to the function proposed by Kaasalainen et al. (2003) and Muinonen et al. (2009), i.e.

$$P_r(\alpha) = A_0 \left[\exp\left(-\frac{\alpha}{A_1} \right) - 1 \right] + A_2 \alpha, \quad (1)$$

where A_0, A_1, and A_2 are constant coefficients. The phase-polarization curve was then used to find α_{min}, α_0, P_{min}, and h. These polarimetric parameters can be used to find the index of refraction n, and the product of the wave number, k, and the mean scatter separation distance, d, applying the procedure used by Gil-Hutton & García-Migani (2017) in the expressions for α_{min} and α_0 proposed first by Shkuratov (1989) and later also used to discuss polarimetry results for miscellaneous random media of scatterers (Muinonen et al. 2002b). This expression is a convenient approximation which makes it possible to obtain physically meaningful parameters within the interference mechanism, although there are other possible mechanisms capable of producing negative polarization (Shkuratov et al. 1994). Table 2 lists for these 20 asteroids the values of α_{min} and its error, P_{min} and its error, α_0 and its error, h and its error, n, kd, and the Bus taxonomic classification. It is important to mention that the asteroids (41) Daphne, (119) Althaea, (130) Elektra, (200) Dynamene, (237) Coelestina, (243) Ida, (503) Evelyn, and (863) Benkoela, included in Table 2, are objects that do not reach phase angles larger than ≈21° because their orbits have semi-major axes larger than ≈2.7 au, therefore it is not possible to observe these asteroids for phase angles larger than the inversion angle. Nevertheless, in these cases the phase-polarization curve obtained is sufficient to define useful polarimetric parameters.

On the other hand, the data obtained allowed us to find tentative phase-polarization curves and polarimetric parameters for the asteroids (52) Europa, (57) Mnemosyne, (72) Feronia,

[3] The catalog is available on the web page of the Grupo de Ciencias Planetarias at http://gcpsj.sdf-eu.org/catalogo.html

Table 2. New asteroids with polarimetric parameters and values of n and kd.

Asteroid	$\alpha_{\min}$ °	$\sigma_{\alpha_{\min}}$ °	$P_{\min}$ %	$\sigma_{P_{\min}}$ %	α_0 °	σ_{α_0} °	h %/°	σ_h %/°	n	kd	Tax
(26) Proserpina	8.78	0.86	−0.685	0.147	19.56	0.35	0.1139	0.0095	1.732	11.234	S
(37) Fides	6.94	1.29	−0.743	0.296	20.24	0.51	0.0788	0.0149	1.740	21.058	S
(41) Daphne	10.40	1.38	−1.512	0.430	22.57	0.17	0.2288	0.0240	1.858	9.067	Ch
(43) Ariadne	8.92	0.64	−0.444	0.078	20.16	0.57	0.0699	0.0037	1.754	11.323	Sk
(49) Pales	9.29	1.59	−1.823	0.700	21.34	0.15	0.2636	0.0353	1.799	11.168	Ch
(93) Minerva	8.66	1.18	−1.070	0.316	18.47	0.20	0.2041	0.0219	1.695	10.563	C
(119) Althaea	8.96	1.25	−0.673	0.212	19.46	0.34	0.1179	0.0127	1.732	10.537	Sl
(130) Elektra	8.24	1.65	−1.960	0.853	21.96	0.18	0.2171	0.0453	1.812	15.707	Ch
(200) Dynamene	9.80	0.45	−1.863	0.195	21.48	0.14	0.2903	0.0105	1.812	9.789	Ch
(216) Kleopatra	7.71	0.55	−0.964	0.158	21.73	0.40	0.0998	0.0072	1.800	18.139	Xe
(237) Coelestina	8.14	1.97	−0.643	0.346	19.56	0.43	0.0939	0.0199	1.724	13.681	S
(243) Ida	8.31	1.23	−0.691	0.239	18.03	0.31	0.1307	0.0144	1.675	11.342	S
(268) Adorea	8.97	0.93	−1.165	0.260	19.25	0.19	0.2106	0.0173	1.726	10.308	X
(345) Tercidina	9.83	0.96	−1.468	0.314	21.06	0.16	0.2435	0.0180	1.799	9.382	Ch
(354) Eleonora	8.80	1.44	−0.483	0.170	19.35	0.48	0.0831	0.0121	1.726	10.959	Sl
(374) Burgundia	4.13	0.63	−0.830	0.107	19.60	0.66	0.0602	0.0070	1.710	62.492	S
(503) Evelyn	11.01	1.36	−1.241	0.358	24.14	0.23	0.1723	0.0159	1.920	8.718	Ch
(757) Portlandia	4.84	0.85	−1.052	0.251	16.19	0.34	0.1192	0.0074	1.583	35.939	Xk
(863) Benkoela	7.91	0.69	−0.464	0.110	18.27	0.52	0.0775	0.0067	1.677	13.222	A
(1627) Ivar	10.25	4.40	−0.362	0.333	21.47	0.65	0.0615	0.0207	1.820	8.638	S

Table 3. Mean values of the polarimetric parameters, n and kd for different taxonomic types.

Asteroid	N	$\alpha_{\min}$ °	$\sigma_{\alpha_{\min}}$ °	$P_{\min}$ %	$\sigma_{P_{\min}}$ %	α_0 °	σ_{α_0} °	h %/°	σ_h %/°	n	σ_n	kd	σ_{kd}
A	2	6.92	2.06	−0.511	0.09	18.71	0.80	0.0610	0.0216	1.69	0.02	29.51	23.03
B	12	7.91	0.86	−1.320	0.20	18.10	1.49	0.2305	0.0244	1.67	0.06	12.93	2.63
C	8	8.22	0.99	−1.535	0.22	19.40	1.27	0.2521	0.0344	1.72	0.05	11.79	2.51
Cb	6	7.90	0.96	−1.231	0.24	17.69	2.13	0.2279	0.0463	1.66	0.08	12.87	2.58
Ch	15	9.64	0.57	−1.647	0.23	21.36	0.87	0.2580	0.0332	1.81	0.04	10.26	1.85
L	4	8.18	1.89	−0.794	0.05	20.12	1.97	0.1116	0.0223	1.75	0.09	14.37	6.42
Ld	2	6.41	0.43	−0.771	0.24	16.63	3.57	0.1208	0.0148	1.62	0.13	19.36	2.77
K	3	9.75	0.94	−0.846	0.46	21.96	2.32	0.1422	0.0588	1.81	0.09	9.53	0.78
R	1	7.94	0.00	−0.368	0.00	20.03	0.00	0.0485	0.0000	1.74	0.00	15.07	0.00
S	25	7.83	1.31	−0.714	0.10	20.47	1.14	0.0886	0.0191	1.76	0.04	16.65	10.43
Sa	2	8.28	0.45	−0.777	0.10	20.71	1.52	0.1000	0.0228	1.77	0.06	14.23	0.41
Sk	3	8.25	0.56	−0.608	0.18	19.76	0.70	0.0861	0.0200	1.74	0.03	13.65	2.02
Sl	10	7.91	1.13	−0.670	0.16	20.08	1.29	0.0938	0.0140	1.74	0.05	14.83	5.07
T	1	9.18	0.00	−0.754	0.00	23.26	0.00	0.0849	0.0000	1.87	0.00	13.12	0.00
V	3	7.62	0.75	−0.654	0.09	20.04	1.46	0.0706	0.0203	1.76	0.05	13.41	5.95
X	9	8.28	0.97	−1.032	0.16	20.32	1.07	0.1318	0.0538	1.77	0.04	14.56	5.62
Xc	7	7.26	2.15	−0.706	0.51	19.51	1.76	0.1020	0.0904	1.70	0.09	20.02	17.38
Xe	8	6.89	1.21	−0.515	0.38	19.84	2.11	0.0654	0.0400	1.71	0.08	19.18	8.93
Xk	3	8.50	2.04	−1.289	0.14	20.00	3.90	0.1440	0.0576	1.75	0.18	19.96	13.98
Bar	5	12.21	0.80	−1.410	0.16	28.46	1.69	0.1512	0.0478	2.11	0.06	9.27	2.53

Notes. The Barbarians are indicated as Bar-type.

(94) Aurora, (96) Aegle, (118) Peitho, (313) Chaldaea, (339) Dorothea, (350) Ornamenta, (357) Ninina, (381) Myrrha, (402) Chloe, (455) Bruchsalia, (471) Papagena, and (579) Sidonia. This increases to 50 the objects in the catalog for which phase-polarization curves and polarization parameters of very good quality can be obtained with very few new observations.

Among the 135 asteroids with a phase-polarization curve of good quality included in the catalog there are 129 with a Bus taxonomic classification. Therefore it is possible to use their polarimetric parameters to find mean values for the different taxonomic types. Table 3 lists for 19 taxonomic types and the Barbarians the number of objects with known polarimetric parameters in that type, and the mean value of $\alpha_{\min}$, $P_{\min}$, α_0, h, n, kd, and their errors. In agreement with the results of Cañada-Assandri et al. (2012), the largest errors appear for X-class types because the Bus taxonomy does not take into account the albedo of the asteroids; in each of these types there are mixed objects classified as E-, M-, and P-type in the Tholen taxonomy (Tholen 1989), which have different albedo and polarimetric properties. There are also several taxonomic types with only 1 or 2 objects with known polarimetric parameters, such as A-, R- or T-type, for which their mean values must be taken with care until more objects of these types are included.

Adding the data for the asteroids with polarimetric parameters of good quality, along with the data of objects with a tentative phase-polarization curves good enough to obtain

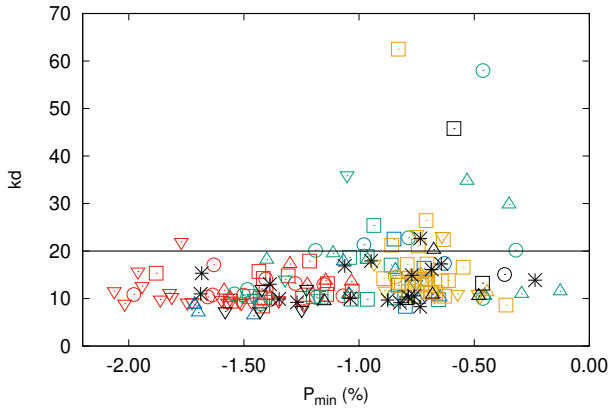

Fig. 1. Relation between $P_{\rm min}$ and kd for 169 asteroids. The B-type objects are indicated with red squares, C-type with red circles, Cb-type with red triangles, Ch-type with red inverted triangles, L-type with blue squares, Ld-type with blue circles, K-type with blue triangles, T-type with blue inverted triangles, X-type with green squares, Xc-type with green circles, Xe-type with green triangles, Xk-type with green inverted triangles, S-type with yellow squares, Sa-type with yellow circles, Sk-type with yellow triangles, Sl-type with yellow inverted triangles, A-type with black squares, R-type with black circles, V-type with black triangles, the Barbarians with black inverted triangles, and those objects without taxonomic type in the Bus taxonomy with black stars.

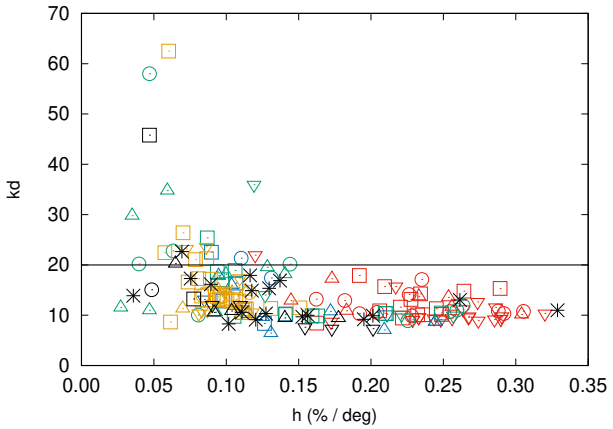

Fig. 2. Relation between h and kd for 169 asteroids. The objects are indicated with the same codification indicated in Fig. 1.

acceptable polarimetric parameters, results in a total of 169 asteroids with data that can be used to search for correlations between the polarimetric parameters, n, kd and the orbital elements. In general, no significant correlations appear between these parameters with the exception of the known correlations $\alpha_{\rm min}$ vs. kd and α_0 versus n (Gil-Hutton & García-Migani 2017), but it is possible to obtain interesting results from plots of kd against $P_{\rm min}$, h, and the perihelion distance, q.

Figures 1–3 show the relations between kd and $P_{\rm min}$, h, and q, respectively. Taking into account that the observations used for these calculations were made in V band, the scatter separation distance obtained is between 1 and 6 μm with a significant concentration for $d \leq 2$ μm, but ~10% of the objects have $d > 2$ μm and they are concentrated in the regions $|P_{\rm min}| < 1\%$, $h < 0.12{-}0.15\%/^\circ$ and $1.8 < q < 2.5$ au. The first two conditions indicate that the asteroids with large kd are possibly those with high or moderate albedos, and the third condition indicates that these objects seem to have perihelion distances in the inner

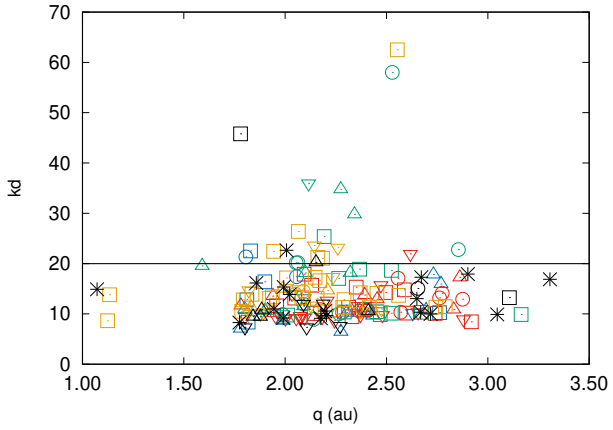

Fig. 3. Relation between q and kd for 169 asteroids. The objects are indicated with the same codification indicated in Fig. 1.

region of the asteroid belt below the 3:1 mean motion resonance with Jupiter. The taxonomic types of these objects are mainly S- or X-class, which also agrees with what is expected in the inner belt.

To better understand this group of asteroids at high values of kd we calculated the mean scatter separation distance for spherical particles of the same size, which are in contact with each other and resting at the surface. The results obtained indicate that the mean scattering distance between two particles is about half the radius of the particles. Thus to have a mean distance between the scatters of $d \approx 1.5$ μm or $d \approx 5$ μm, the particles should have radii of ≈ 3 or ≈ 10 μm, respectively. The former case represent the ~90% of the objects in Figs. 1–3, which could mean that most regoliths are composed of relatively fine particles, while the second case suggests the presence of larger particles on the surface of the remaining objects. In fact, the returned regolith sample of the asteroid (25143) Itokawa reveals that most particles range from 10 to 50 μm in size (Nakamura et al. 2011). But Itokawa is a rubble pile and a very small Apollo object whose regolith could lose the fine particles produced by micro-collisions owing to several physical processes.

It is also possible to propose a different scenario to explain the ~10% of the objects with large particle separations if the electrostatic forces acting over the small grains of the regolith are taken into account. As is well known, the surfaces of asteroids are exposed to solar wind plasma and solar UV radiation, resulting in a positive surface potential (Mendis et al. 1981; Lee 1996). These effects could contribute to the generation of two important currents over the surface, which are responsible for developing a photoelectron sheath over the lit side. Since the upper layer of the regolith on a small body may be considered as an effective insulator, the regolith dust particles has a non-zero charge while resting on the surface and, under certain conditions, the electric force on small particles would exceed the gravitational force causing dust particles to detach from the surface or, at least, separate from each other. This mechanism has been used to explain the smooth flat deposit seen on (433) Eros (Robinson et al. 2001; Hughes et al. 2008) and the horizon glow on the Moon (Criswell 1972) caused by fine particles of the lunar regolith (Greenberg et al. 2007).

To test this hypothesis, we run a simulation of the electrostatic process on asteroids following the simplified, monotonically decreasing sheath potential model described by Colwell et al. (2005) and Hughes et al. (2008). This model assumes that the solar UV radiation strikes the surface and releases electrons

of at least the same energy of the incoming photons; at the same time the solar wind hits the surface, thereby producing an electron current. If the photoemission process results to be more effective than the solar wind charging process, then the sunlit surface becomes positively charged. On the other hand, dust grains also release electrons through the photoelectric effect, and collect solar wind electrons and photoelectrons from the photoelectron sheath in a similar way as happens on the surface. This process is time dependent and results in a variation of the grain charge, which in turn produces repulsion between the grain and the surface which, in the case in which it overcomes the force of gravity, produces the separation of the particles from the surface.

As mentioned previously, the particle charging mechanism is determined by the currents over the surface. Therefore, to calculate the photoelectron currents arrived at and emitted from the grains we assumed that the asteroid surfaces have photoemissive properties similar to the lunar regolith. Then, the photocurrent at a distance d (in au) from the Sun is $I_{\rm ph0} = 5.88 \times 10^9/d^2$ electrons $(\mathrm{cm^2 s})^{-1}$ (Willis et al. 1973; Senshu et al. 2015) and the average photoelectron temperature measured for a lunar regolith is $\kappa_{\rm B} T_{\rm pe} = 2.2\,\mathrm{eV}$ (Willis et al. 1973). For the solar wind current, however we assumed that the solar wind electron density is constant at a given distance of the Sun, $n_{\rm sw} \approx 5/d^2$ electrons $\mathrm{cm^{-3}}$ (Mendis et al. 1981) and that the solar wind electron temperature is $\kappa_{\rm B} T_{\rm sw} = 10\,\mathrm{eV}$. In our case we also assumed an asteroid gravity of $0.5 \times 10^{-2}\,\mathrm{m\,s^{-2}}$ that is equivalent to that of Eros and a heliocentric distance of 2.5 au. We calculated the electric and gravity forces acting on a mesh of 10×10 particles of $0.4\,\mu$m in radius resting on the surface of the asteroid; these particles are the candidates to be lifted from the surfaces by levitation. If the initial mean scatter separation distance on the surface was on the order of 1 μm or less, we find that these particles detach from the surface after a short time and begin to levitate reaching a mean separation between the particles of ≈ 5 μm, which corresponds to the high values of kd found in this paper. Then, it is also possible to understand the high values of kd observed on some asteroids as a consequence of the presence of a cloud of levitating fine regolith particles over their surfaces produced by an electrostatic repulsion process.

There are also other possibilities to explain these objects. Since a shift of polarization minima toward small phase angles are directly related with large kd (Gil-Hutton & García-Migani 2017), it is possible to assume that it could be a manifestation of the coherent backscattering mechanism similar to that observed in high albedo objects (Mishchenko et al. 2006) or perhaps a result of a surface formed by dark and bright particles (Bagnulo et al. 2006). But to discern the acting mechanism with confidence, it will be necessary to detect and study more objects with large kd.

4. Conclusions

Using the CASPOL polarimeter at Complejo Astronómico El Leoncito, we obtained 128 polarimetric measurements for 82 main-belt asteroids of different taxonomic types. The asteroids (107) Camilla, (307) Nike, and (346) Hermentaria were observed for the first time.

The observational data allowed us to find phase-polarization curves and polarimetric parameters for 20 asteroids, reaching a total of 135 objects with sufficient good data in the Catalogue of Asteroid Polarization Curves. Using the values obtained for 129 objects classified in the taxonomy of Bus (1999), the mean polarimetric parameters for 18 taxonomic types and the Barbarians were obtained. On the other hand, the data obtained allow us to find tentative polarization parameters for 15 asteroids not included previously in the catalog.

No significant correlations appear between the polarimetric parameters, n, kd and the orbital elements, with the exception of the known correlations $\alpha_{\rm min}$ vs. kd and α_0 versus n (Gil-Hutton & García-Migani 2017), but the asteroids with large kd have $|P_{\rm min}| < 1\%$, $h < 0.12{-}0.15\%/^\circ$ and $1.8 < q < 2.5$ au, indicating they have high or moderate albedos and perihelion distances in the inner region of the asteroid belt. These large kd values could be the result of an electrostatic mechanism acting on the small grains of the regolith, thereby producing dust particles to detach from the surface and separate each other. This could be a manifestation of a coherent backscattering mechanism or the result of a surface formed by a mixture of dark and bright particles, but in any case objects with large values of kd must be the subject of deeper studies in the future.

Acknowledgements. The authors gratefully acknowledge financial support by CONICET through PIP 112-201501-00525 and San Juan National University by a CICITCA grant for the period 2018-2019.

References

Bagnulo, S., Boehnhardt, H., Muinonen, K., et al. 2006, A&A, 450, 1239
Bus, S. J. 1999, Ph.D. Thesis, Massachusetts Institute of Technology, USA
Bus, S. J., & Binzel, R. P. 2002, Icarus, 158, 146
Cañada-Assandri, M., Gil-Hutton, R., & Benavidez, P. 2012, A&A, 542, A11
Colwell, J. E., Gulbis, A. A. S., Horányi, M., & Robertson, S. 2005, Icarus, 175, 159
Criswell, D. R. 1972, Lunar Planet. Sci. Conf. Proc., 3, 2671
Dollfus, A., Wolff, M., Geake, J. E., Dougherty, L. M., & Lupishko, D. F. 1989, in Asteroids II, eds. R. P. Binzel, T. Gehrels, & M. S. Matthews (Tucson: University of Arizona Press), 594
Fornasier, S., Belskaya, I. N., Shkuratov, Y. G., et al. 2006, A&A, 455, 371
Fossati, L., Bagnulo, S., Mason, E., & Landi Degl'Innocenti, E. 2007, in The Future of Photometric, Spectrophotometric and Polarimetric Standardization, ed. C. Sterken, ASP Conf. Ser., 364, 503
Gil-Hutton, R., & Benavidez, P. 2003, MNRAS, 345, 97
Gil-Hutton, R., & García-Migani, E. 2017, A&A, 607, A103
Gil-Hutton, R., López-Sisterna, C., & Calandra, M. F. 2017, A&A, 599, A114
Greenberg, P. S., Chen, D., & Smith, S. A. 2007, Aerosol Measurements of the Fine and Ultrafine Particle Conten of Lunar Regolith
Hughes, A. L. H., Colwell, J. E., & DeWolfe, A. W. 2008, Icarus, 195, 630
Kaasalainen, S., Piironen, J., Kaasalainen, M., et al. 2003, Icarus, 161, 34
Lazzaro, D., Angeli, C. A., Carvano, J. M., et al. 2004, Icarus, 172, 179
Lee, P. 1996, Icarus, 124, 181
Magalhaes, A. M., Rodrigues, C. V., Margoniner, V. E., Pereyra, A., & Heathcote, S. 1996, in Polarimetry of the Interstellar Medium, eds. W. G. Roberge & D. C. B. Whittet, ASP Conf. Ser., 97, 118
Mendis, D. A., Hill, J. R., Houpis, H. L. F., & Whipple, E. C. 1981, ApJ, 249, 787
Mishchenko, M. I., Rosenbush, V. K., & Kiselev, N. N. 2006, Appl. Opt., 45, 4459
Muinonen, K., Piironen, J., Shkuratov, Y. G., Ovcharenko, A., & Clark, B. E. 2002a, in Asteroids III, eds. W. F. Bottke, Jr. A. Cellino, P. Paolicchi, & R. P. Binzel (Tucson: University of Arizona Press), 123
Muinonen, K., Videen, G., Zubko, E., & Shkuratov, Y. 2002b, in Optics of Cosmic Dust, eds. G. Videen & M. Kocifaj (Berlin: Springer Science & Business Media), 261
Muinonen, K., Penttilä, A., Cellino, A., et al. 2009, Meteorit. Planet. Sci., 44, 1937
Nakamura, T., Noguchi, T., Tanaka, M., et al. 2011, Science, 333, 1113
Robinson, M. S., Thomas, P. C., Veverka, J., Murchie, S., & Carcich, B. 2001, Nature, 413, 396
Senshu, H., Kimura, H., Yamamoto, T., et al. 2015, Planet. Space Sci., 116, 18
Shkuratov, I. G. 1989, Astronomicheskii Vestnik, 23, 176
Shkuratov, Y. G., Muinonen, K., Bowell, E., et al. 1994, Earth Moon Planets, 65, 201
Tholen, D. J. 1989, in Asteroids II, eds. R. P. Binzel, T. Gehrels, & M. S. Matthews (Tucson: University of Arizona Press), 1139
Turnshek, D. A., Bohlin, R. C., Williamson, II, R. L., et al. 1990, AJ, 99, 1243
Willis, R. F., Anderegg, M., Feuerbacher, B., & Fitton, B. 1973, Astrophys. Space Sci. Lib., 37, 389